land

MDPI

Article

Regional and Phased Vegetation Responses to Climate Change Are Different in Southwest China

Meng Wang [1,*] and Zhengfeng An [2]

[1] Chaozhou Environmental Information Center, Chaozhou 521011, China
[2] Department of Renewable Resources, University of Alberta, Edmonton, AB T6G 2E3, Canada; za2@ualberta.ca
* Correspondence: wangmengzhisha@126.com

Abstract: Southwestern China (SW) is simultaneously affected by the East Asian monsoon, South Asian monsoon and westerly winds, forming a complex and diverse distribution pattern of climate types, resulting in a low interpretation rate of vegetation changes by climate factors in the region. This study explored the response characteristics of vegetation to climatic factors in the whole SW and the core area of typical climate type and the phased changes in response, adopting the form of "top-down", using linear trend method, moving average method and correlation coefficient, and based on the climate data of CRU TS v. 4.02 for the period 1982–2017 and the annual maximum, 3/4 quantile, median, 1/4 quantile, minimum and average (abbreviated as P_{100}, P_{75}, P_{50}, P_{25}, P_5 and Mean) of GIMMS NDVI, which were to characterize vegetation growth conditions. Coupling with the trend and variability of climate change, we identified four major types of climate change in the SW, including the significant increase in both temperature and precipitation (T^{+*}-P^{+*}), the only significant increase in temperature and decrease (T^{+*}-P^{-}) or increase (T^{+*}-P^{+}) of precipitation and no significant change (NSC). We then screened out nine typical areas of climate change types (i.e., core areas (CAs)), followed by one T^{+*}-P^{+*} area, which was located in the center of the lake basin of the Qiangtang Plateau. The response of vegetation to climatic factors in T^{+*}-P^{+*} area/T^{+*}-P^{+} areas and T^{+*}-P^{-} areas/NSC areas were mainly manifested in an increase and a significant decrease, which makes the response characteristics of vegetation to climatic factors in the whole SW have different directionality at different growth stages. Our results may provide new ideas for clearly showing the complexity and heterogeneity of the vegetation response to climate change in the region under the background of global warming.

Keywords: Southwestern China; typical climate types; regional and phased responses; multiple correlations

Citation: Wang, M.; An, Z. Regional and Phased Vegetation Responses to Climate Change Are Different in Southwest China. *Land* **2022**, *11*, 1179. https://doi.org/10.3390/land11081179

Academic Editors: Isa Ebtehaj and Babak Mohammadi

Received: 28 June 2022
Accepted: 25 July 2022
Published: 28 July 2022

1. Introduction

Since the 1980s, with the development of satellite remote sensing technology, many continuously changing remote sensing data have been captured worldwide [1]. A large number of studies on eco-environmental changes at watershed and landscape scales have been successfully applied to analyze the correlation between vegetation change and global climate and environmental factors and achieved fruitful results (e.g., [2–10]). Many studies have shown that vegetation growth is closely related to climate conditions, and climate can determine vegetation growth and development through spatial and temporal redistribution [11–13]. In particular, the temporal variability of precipitation and potential evapotranspiration have profound effects of vegetation growth and phenology [14]. Moreover, it is well-acknowledged that future climate projection will highly affect forest growth and even forest line shift [15]. Climate warming has caused significant changes in vegetation cover both regionally and globally, especially in cold ecosystems, where the temperature is an important limiting factor, which plays a leading role in vegetation growth in northern high latitudes (e.g., [2,4,16]), and warming significantly enhanced vegetation activity [17,18].

Precipitation has a great influence on *NDVI* at the regional scale, and there is usually a positive correlation between *NDVI* and precipitation [19–21]. Especially in arid and semi-arid areas, water availability is the key to vegetation growth, and more precipitation will promote vegetation restoration, such as the Eurasian (>23.5° N) and the arid and semi-arid areas in the upper reaches of the Yarlung Zangbo River Basin, where precipitation has a positive impact on vegetation greening [13,19]. Excessive water may inhibit the growth of vegetation, which the increase of precipitation in the humid arid transition zone of northern China promotes the growth of vegetation in drier areas with sparse vegetation, and inhibits the growth of vegetation in humid areas with high vegetation coverage [22]. Forest vegetation in Southeast Asia is positively correlated with precipitation in the dry season, but is not sensitive to precipitation in the rainy season [23].

Moreover, vegetation growth is usually affected by climatic factors in the spatiotemporal scale, of which temperature and precipitation are the main factors controlling global vegetation growth, and the temporal trend of spatial heterogeneity of climate factors may lead to more complex responses of vegetation activities [8,24–26]. This is especially true since 1850, and every decade of the last 40 years has been consecutively warmer than any previous decade, and further forecasts predict that climate change in the coming decades will intensify the water cycle and water imbalances, bringing more rainfall and flooding, and more severe droughts [27]. Some studies have pointed out that the global vegetation greenness was significantly reduced due to increased temperature and the decrease in precipitation. In the past decade, greening in the Northern Hemisphere seems to have stopped, and browning has gradually become the main trend [8,24,26]. In the Qinghai-Xizang Plateau, the cold and dry environment is extremely sensitive to climate change, and vegetation growth is controlled by both water supply and temperature increase [21]. The response of vegetation activity to temperature in the growing season is positively regulated by precipitation, and the positive response to precipitation may be enhanced by temperature rise, especially for alpine grasslands in relatively arid areas [28]. At the same time, some studies have shown that the response of vegetation activities to climate change changes with time, and the correlation calculated based on one period cannot be simply applied to another period [4,8,29]. During the 1980s and 1990s, global warming led to a significant increase in vegetation activities [30], and then, since the mid-1990s, the global vegetation browning trend has been accelerating, and in the area north of 30° N, the stimulation effect of temperature increase is weakening [4,8,29,31].

With the in-depth research development, quantifying the relationship between vegetation growth and climate change has gradually become a central topic and challenge in the current global change research. Some related studies have reported the response of vegetation growth to climate driving factors at different scales [3,5,6,8,10,18,26,28]. These studies usually use the interannual variation of the maximum value in the year or in the growing season to characterize the growth and change of vegetation. Compared with different periods of vegetation growth, the performance between the maximum value and climate factors is also different [32]; interannual changes are used to characterize changes in vegetation growth, which are easily disturbed by some abnormal values. According to the sliding average method, local averaging can be performed to obtain a relatively smooth new *NDVI* time series, which is conducive to more intuitively presenting the changing trend of vegetation [33]; and affected by different climatic factors, the corresponding response is also different, which changes with time.

The SW is the most complex region in China, across the three steps of China's terrain, affected by the East Asian monsoon, South Asian monsoon and westerly wind, resulting in the formation of a more complex and diverse distribution pattern of climate types [34–37]. Global climate warming [38,39] makes the growth and distribution pattern of vegetation more sensitive to climate change [18,40,41]; thus, we put forward the scientific questions of this study: (1) How to reveal the major types of climate change in SW and further identify the typical areas of climate change types? (2) How to characterize and quantify the regional and periodic responses of vegetation to climate factors.

2. Materials and Methods

Thus, to improve the understanding of vegetation response to climate change, the climate change types existing in SW were revealed from the aspects of climate change trend (rate, direction, significance and probability) and variability, and the typical areas of climate change types (i.e., core areas (CAs)) were selected. The value was selected P_{100}, P_{75}, P_{50}, P_{25}, P_5 and Mean of GIMMS NDVI, which was generated by choosing the 15-year sliding step size, to characterize vegetation growth conditions [42]. The dynamic law of vegetation growth in SW and the CA was explored in the form of "top-down", and the response characteristics of vegetation to climate factors and their periodic changes were deeply discussed, to understand the response process of vegetation to climate factors in SW in recent decades.

2.1. Study Region

Under the natural zoning concept [34], the "Southwestern China Region" is referred to in this research with a broader geographical implication and consideration of vegetation and landscape settings, covering Sichuan, Chongqing, Guizhou, and Yunnan in the entirety, and parts of Xizang and Qinghai (Figure 1a). The whole study area spanned coordinates between 21.14° and 36.48° N, and 83.87° and 110.19° E, and mean annual temperature of 5.76 °C and mean annual precipitation of 768.4 mm for the period 1901–2017 [37], covering the Himalaya Mountains, the eastern Qinghai-Xizang Plateau, the Hengduan Mountains, Zoige Plateau, Sichuan Basin, Yunnan-Guizhou Plateau and other terrain units, and the unique climate of Qinghai-Xizang Plateau, which have a significant impact on the regional and global climate of East Asia [35,36], has become the focus area of scholars at home and abroad [35,43].

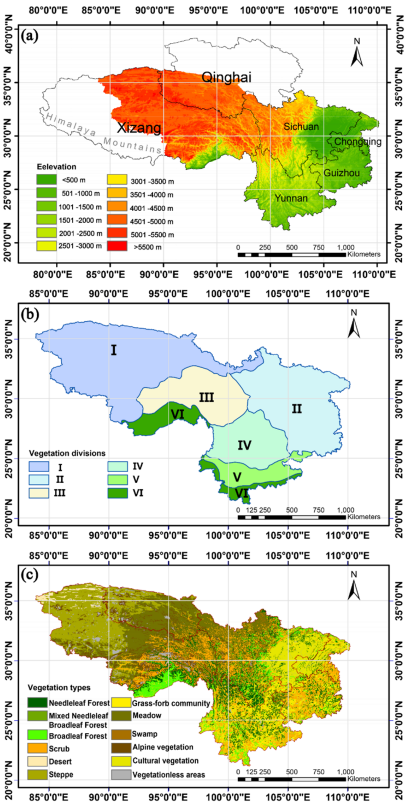

Figure 1. Overview of (**a**) topography, (**b**) vegetation divisions and (**c**) vegetation types in part of southwestern China. The clear space in panel (**a**) are areas within the respective provincial territory not included in this study. Vegetation divisions: I, alpine vegetation region; II–V, respectively, represent the northwest region, west central region and northwest region of subtropical evergreen broad-leaved forest; and VI, tropical monsoon forest.

2.2. Data Sources and Processing

The digital elevation model with a resolution of 1 km (Table 1, https://www.resdc.cn/data.aspx?DATAID=123, accessed on 28 September 2019) was used to obtain the altitude of the SW, and was resampled to 0.25° × 0.25° resolution raster data based on bilinear interpolation extrapolation in ArcGIS10.6, so that the new output grid value was a weighted average of the four closest values from the input cell center, thus obtaining a smoother surface.

Table 1. The main data sources.

Data	Data Sources	Resolution	Data Accessibility Links	Access Date	Access Format
GIMMS $NDVI_{3g}$	GIMMS	8 × 8 km	https://ecocast.arc.nasa.gov/data/pub/GIMMS/	18 November 2018	.nc4
CRU_TS4.02	Climate Research Unit	0.5° × 0.5°	https://crudata.uea.ac.uk/cru/data/hrg/	28 June 2019	.nc
Global Artificial Impervious Area	Tsinghua university data	30 × 30 m	http://data.ess.tsinghua.edu.cn	31 December 2019	.tif
Digital elevation model	Resource and Environment Science and Data Center	1 × 1 km	https://www.resdc.cn/data.aspx?DATAID=123	28 September 2019	GRID
China's vegetation zoning data	Resource and Environment Science and Data Center	—	http://www.resdc.cn/data.aspx?DATAID=133	1 December 2017	.shp
1:1 million vegetation map of China	Resource and Environment Science and Data Center	—	https://www.resdc.cn/data.aspx?DATAID=122	1 December 2017	.shp

The high-resolution gridded temperature and precipitation gridded datasets (CRU_TS4.02) were downloaded from the Climate Research Unit, University of Anglia, UK (Table 1, https://crudata.uea.ac.uk/cru/data/hrg/, accessed on 28 June 2019) with the time range covers from 1901 to 2017, and the spatial resolution of 0.5° × 0.5° was used [44], which was frequently used as reliable climate data sources for studying global or regional patterns of climate change and impacts on ecosystems (e.g., [37,45]). Since the study area spans three steps and the terrain is fragmented in the transition zone, the 0.5° × 0.5° resolution may obscure the relationship between climate change and the environment, and was downscaled to 0.25° × 0.25° using the cubic spline interpolation method [46], incorporating the DEM information at 0.25° × 0.25° spatial resolution.

By piecewise linear regression, we obtained that there were significant turning years ($F > F_{0.05}$) for the annual mean temperature and annual precipitation from 1901 to 2017, which were 1954 and 1928, respectively [37]. According to the current results, the northern hemisphere began to rise in the mid-1970s [47,48], especially after 1980 [39,40,48], combined with the longest *NDVI* time series (GIMMS $NDVI_{3g}$) [49], and we chose 1982–2017 as the main research period.

Based on China's vegetation zoning data obtained on the Resource and Environment Science and Data Center (Table 1, http://www.resdc.cn/data.aspx?DATAID=133, accessed on 1 December 2017), it can indicate the regularity of the geographic distribution of vegetation and mainly includes three regions: the alpine vegetation region of Qinghai–Xizang Plateau, subtropical evergreen broad-leaved forest region, tropical monsoon forest and rainforest region, including 13 vegetation zones. The scattered and minor vegetation zones were aggregated into predominant vegetation types prevailing in the local areas, the regional vegetation zoning data were aggregated into six major sub-regions consisting of the alpine vegetation region, the east region, northwest region, west-central region and northwest region of subtropical evergreen broad-leaved forest and tropical monsoon forest (Figure 1b).

The *NDVI* data were from the GIMMS (global inventory monitoring and modeling studies), which were derived from AVHRR remote sensing imagery and covered the period January 1982–December 2015, with the temporal step of 15 d and spatial resolution of 8 × 8 km (Table 1, https://ecocast.arc.nasa.gov/data/pub/GIMMS/, accessed on 18 November 2018). Although the dataset was widely used in global and regional scale vegetation dynamics research after geometric correction, radiometric correction and atmospheric correction [49], due to the high frequency of days with cloud and precipitation in

the study region, further filtering processing is needed to reconstruct the sequence and eliminate cloud interference. Based on the MATLAB R2019a platform, we further combined with Savitzky–Golay filtering and quality control files on 24 periods *NDVI* every year, to form a new *NDVI* sequence [50], hence eliminating the interference of clouds and rainfall weather conditions.

The Maximum Value Composite (MVC) was used to eliminate some of the interference of clouds, atmosphere, and sun altitude. The computations followed the steps of:

$$NDVI_{mi} = Max(NDVI_{mij}) \tag{1}$$

$$\overline{NDVI} = \frac{\sum_{1}^{m}\sum_{1}^{12} NDVI_{mi}}{12 * m} \tag{2}$$

where $NDVI_{mi}$ represents the *NDVI* of the *i*-th month in the *m*-th year (i = 1, 2,..., 12, m = 1, 2,..., 34), $NDVI_{mij}$ refers to the *NDVI* of the *j*-th 15th day of the *i*-th month in the *m*-th year data (j = 1, 2) and $\overline{NDVI}$ refers to the multi-year average *NDVI*. The threshold value of $\overline{NDVI}$ is 0.1, that is, areas with less than this value have very low productivity and are considered to be uncovered by vegetation [51].

The cultivated vegetation in the vegetation type data (Figure 1c) was greatly affected by anthropogenic activities. At the same time, the rapid development of urbanization in recent years has caused the artificial impervious area to increase rapidly, and all need to be eliminated in this study, based on Global Artificial Impervious Area by Tsinghua university data open platform (Table 1, http://data.ess.tsinghua.edu.cn, accessed on 31 December 2019) [52].

To more comprehensively reflect the changing law of vegetation growth conditions, the value was selected the maximum, 3/4 quantile, median, 1/4 quantile, minimum and average values of GIMMS NDVI for 12 months in a year, which were used to represent the annual value synthesizes of vegetation at different stages of growth, denoted as P_{100}, P_{75}, P_{50}, P_{25}, P_5 and Mean in turn. The computations followed the steps of:

$$\text{Mean} = \frac{\sum_{1}^{12} NDVI_{mi}}{12} \tag{3}$$

$$P_{100} = Max(NDVI_{mi}) \tag{4}$$

$$P_5 = Min(NDVI_{mi}) \tag{5}$$

$NDVI_{mi}$ is sorted first and then calculated using Matlab main programming language (b = sort($NDVI_{mi}$));

$$P_{75} = \text{prctile(b, 75)} \tag{6}$$

$$P_{50} = \text{prctile(b, 50)} \tag{7}$$

$$P_{25} = \text{prctile(b, 25)} \tag{8}$$

2.3. Data Analysis

The least square method was performed on the changing trend of climatic factors (annual temperature and annual precipitation) on the pixel scale, and with the slope of the fitting equation indicating the rate of changes, which was calculated as [53].

$$slope = \frac{n\sum_{i=1}^{n} ix_i - \sum_{i=1}^{n} i\sum_{i=1}^{n} x_i}{n\sum_{i=1}^{n} i^2 - \left(\sum_{i=1}^{n} i\right)^2} \tag{9}$$

where, n is the length of the study period, and x_i is the annual average temperature or annual precipitation of the i-th year. When $slope > 0$, it means that the climate during the study period shows a trend of warming or humidification. Otherwise, it shows a trend of cooling or drying. The significance of the climate factor was determined by t-test.

Error probability and variability analysis were combined to characterize the extent of climate influence. The error probability (Pd) of the rate of change of the index was [54]:

$$Pd = \mathrm{erf}\left(\frac{k}{\sigma\sqrt{2}}\right) \tag{10}$$

where k is the rate of change of a certain index and σ is its standard deviation. $Pd \geq 0.95$ is recorded as high probability, $Pd < 0.95$ is recorded as a low probability [55].

Mainly standard deviation (S) and coefficient of variation (CV) are used to express climate variability. Areas that exceed the 95% upper confidence limit of the T-test are recorded as high variability, and otherwise, areas are recorded as low variability. Among them, the standard deviation was used to characterize the variability of temperature, and the coefficient of variation was used to characterize the variability of precipitation because the precipitation varies by 2 orders of magnitude from east to west. The formula as follows:

$$s = \sqrt{\frac{\sum_{1}^{n}(x_i - \overline{x})^2}{n-1}} \tag{11}$$

$$CV = \frac{s}{\overline{x}} \tag{12}$$

where x_i represents the value of the i-th year of an indicator, $\overline{x}$ is the average value of the study period and n is the number of statistical years.

The moving average method was used to remove the impact of some climate data noise, averaging in the local area, reduce the impact of random effects and get a relatively smooth new climate time series, which was conducive to a more intuitive presentation of climate change trend [33]. The moving average formula was:

$$\overline{p_j} = \sum_{i=j}^{i+L-1} \frac{x_i}{L} \tag{13}$$

where L is the sliding step length (referring to Fu [42], we chose the sliding step length as 15 years); i is the serial number, $j = (L-1)/2 + i$.

Based on partial correlation and multiple correlation analysis methods, temperature and precipitation's influence and comprehensive influence on vegetation *NDVI* were revealed. The computations followed the steps of:

$$R_{xy} = \frac{\sum_{1}^{n}(x_i - \overline{x})(y_i - \overline{y})}{\sqrt{\sum_{1}^{n}(x_i - \overline{x})^2}\sqrt{\sum_{1}^{n}(y_i - \overline{y})^2}} \tag{14}$$

$$R_{xy,z} = \frac{R_{xy} - R_{xz}R_{yz}}{\sqrt{(1 - R_{xz}^2)}\sqrt{\left(1 - R_{yz}^2\right)}} \tag{15}$$

$$R_{x,yz} = \sqrt{1 - \left(1 - R_{xy}^2\right)\left(1 - R_{xz,y}^2\right)} \tag{16}$$

where R_{xy} is the correlation coefficient of the x and y variables, x_i and y_i are the values of *NDVI* and climate factors (temperature and precipitation) in the i-th year; $\overline{x}$ and $\overline{y}$ are

the multi-year average of the two variables; n is the number of years. $R_{xy,z}$ is the partial correlation coefficient between the dependent variable x and the independent variable y after the independent variable z is fixe, and the t-test method was used for the significance test. $R_{x,yz}$ is the multiple correlation coefficient between the dependent variable x and the independent variables y and z, and the F test method was used for the significance test.

The driving zoning principles adopted by related scholars [56,57] were used to analyze the driving force of vegetation growth and change. The classification criteria after appropriate corrections were shown in Table 2.

Table 2. Zoning criteria for the impact factors of *NDVI* changes. R_1, the t significance test of partial correlation between *NDVI* and temperature; R_2, the t significance test of partial correlation between *NDVI* and precipitation; R_3, the F significance test of multiple correlations between *NDVI* and temperature and precipitation.

***NDVI* Changes Driving Factors**			**Zoning Criterias**		
			R_1	**R_2**	**R_3**
Climate factors	Changed by temperature and precipitation strongly	$[T+P]^+$	$\|t\| > t_{0.01}$	$\|t\| > t_{0.01}$	$F > F_{0.05}$
	Changed by temperature and precipitation weakly	$[T+P]^-$			$F > F_{0.05}$
	Changed by temperature	T	$\|t\| > t_{0.01}$		$F > F_{0.05}$
	Changed by precipitation	P		$\|t\| > t_{0.01}$	$F > F_{0.05}$
	Changed by temperature weakly	T^-	$t_{0.05} < \|t\| \leq t_{0.01}$		$F > F_{0.05}$
	Changed by precipitation weakly	P^-		$t_{0.05} < \|t\| \leq t_{0.01}$	$F > F_{0.05}$
Non-climate factors	Changed by non-climate	NC			$F \leq F_{0.05}$

The correlation coefficient R_i and complex correlation coefficient FR_i between the *NDVI* series of 1982–1996, 1983–1997, . . . , 2001–2015 and the climatic factors (temperature and precipitation) in the corresponding period, with 15 years as the step [42], referencing Formulas (15) and (16), were used to reconstitute the new sequence, and calculate the changing trend according to the Formula (9), which referred to the change trend of response intensity of vegetation to climatic factors. The significance test was determined by t-test of the new sequence.

All data analysis, unless otherwise specified, was performed using MATLAB R2019a.

3. Results

3.1. Identification of Typical Climate Types in the Past 30 Years

Four types of climate change on the grid scale can be obtained by referring to Table A1, which were the areas with a significant increase in temperature and precipitation (abbreviated as T^{+*}-P^{+*}), the areas with a significant increase of temperature was related to the decrease of precipitation (abbreviated as T^{+*}-P^{-}), the areas with a significant increase of temperature was related to the increase of precipitation (abbreviated as T^{+*}-P^{+}) and no significant change (abbreviated as NSC) (Figure 2a). In terms of the spatial coverage, about half of the region were of the type T^{+*}-P^{+}, 34.22% the type T^{+*}-P^{-}, 15.13% the type T^{+*}-P^{+*} and 1.9% of the region were not detected with a clear trend of climate change (NSC).Values were assigned according to Table A2, and divided into four categories according to the scores, which were respectively marked as slight, mild, and moderate and intensive to get the spatial distribution of climate influence degree on the grid scale in the SW region (Figure 2b).

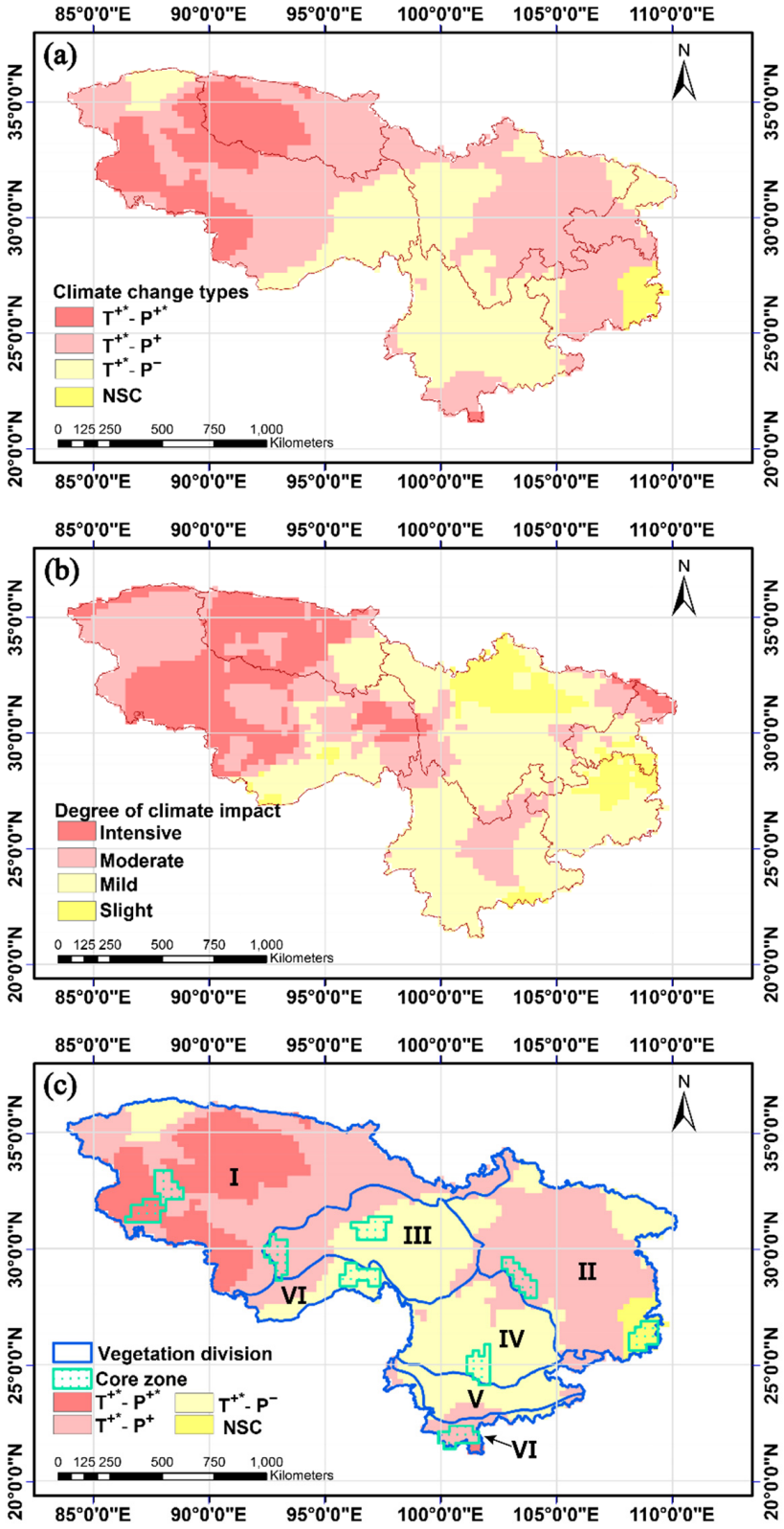

Figure 2. (**a**) Spatial distributions of climate change types, (**b**) the degree of climate impact and (**c**) the core region of the climate change model in the study region of southwestern China. Climate change types: T^{+*}-P^{+*}, the type with a significant increase in temperature and precipitation; T^{+*}-P^{-}, the type with a significant increase of temperature was related to the decrease of precipitation; T^{+*}-P^{+}, the type with a significant increase of temperature was related to the increase of precipitation; NSC, the type with no significant change."+/−" means an increase/decrease in temperature or precipitation; "*" significant at $p < 0.05$.

Based on the principles of homogeneity (Table A3, Figure A1a and see Appendix A(1) for details), typicality (Figure A1b and see Appendix A(2) for details) and concentration (see Appendix A(3) and Appendix A(4) for details), the typical regions of climate change types (i.e., core regions (CAs)) were selected (Figure 2c). For the specific steps, please refer to Appendix B. In the CAs, the trend and volatility of climate change were consistent, which can explain the inconsistent rules of climate change in the study area. Finally, nine CAs were selected, which were: one T^{+*}-P^{+*} area, located in the center of Qiangtang plateau lake basin three T^{+*}-P^{-} areas, which were located in the center of the high mountains and deep valleys in eastern Xizang, the easternmost part of the southern limb of the eastern Himalayas and some centers of Yunnan in Yunnan–Guizhou Plateau; four T^{+*}-P^{+} areas in the north of the lake basin center of Qiangtang plateau, the west of the mountains and valleys in Southeast Xizang, the southwest of Sichuan Basin and the south of Yunnan-Guizhou Plateau; and one NSC area was located in the southeast part of Guizhou Province in Yunnan–Guizhou Plateau.

3.2. Characteristics of Vegetation Changes in Core Areas

In this analysis, the interannual variation of vegetation growth was analyzed with a 15-year sliding step by referring to Fu [42]. The average value of *NDVI* in the southwest and different core areas was in the following order: NSC > T^{+*}-P^{-} > T^{+*}-P^{+} > SW > T^{+*}-P^{+*} (Figure 3), the smallest in the T^{+*}-P^{+*} area, and the six growth stages were less than 2500.00×10^{-4}, the largest in the NSC area, all over 5500.00×10^{-4}. *NDVI* in the SW, T^{+*}-P^{-}, T^{+*}-P^{+} and NSC area general increased significantly ($p < 0.01$), whereas a significant decreasing trend was showed in the T^{+*}-P^{+*} area ($p < 0.01$). The results showed that the overall scope and growth stage of the SW region displayed a significant increasing trend, which covered the significant decreasing trend of vegetation in the T^{+*}-P^{+*} areas and the significant decreasing trend in P_{75} in the T^{+*}-P^{+} area and P_5 in the NSC area, which further showed that the vegetation in the SW region was improving as a whole, and there was a risk of deterioration in some parts; at the same time, there was the possibility that local areas will deteriorate in a specific period.

Furthermore, we found that the difference in k between the SW and the CAs was noticeable. The order of the multi-year average k value of the six annual values was basically: NSC > T^{+*}-P^{+} > T^{+*}-P^{+*} > SW > T^{+*}-P^{-} (Figure 3). The trend of k (similar to the acceleration in physics, abbreviated as ka) in the SW region, T^{+*}-P^{+*} and T^{+*}-P^{-} areas mostly showed a significant decrease ($p < 0.01$), T^{+*}-P^{+} areas showed a decreasing trend, and the 6 growth stages in the T^{+*}-P^{-} areas showed the fastest rate of decrease, which was approximately 2.72–11.54 times the decrease rate in the SW region. There was a slight increase trend in T^{+*}-P^{+*} and T^{+*}-P^{+} areas, but they had not reached a significant level; in the NSC area, there was a significant increasing trend. It showed that the overall range and growth stage of the change trend k in the SW region revealed a significant decrease trend, covering up the significant increasing trend of vegetation in the NSC area and the T^{+*}-P^{+*} area at P_5 and P_{25} and the T^{+*}-P^{+} area at P_{50} and P_{75}.

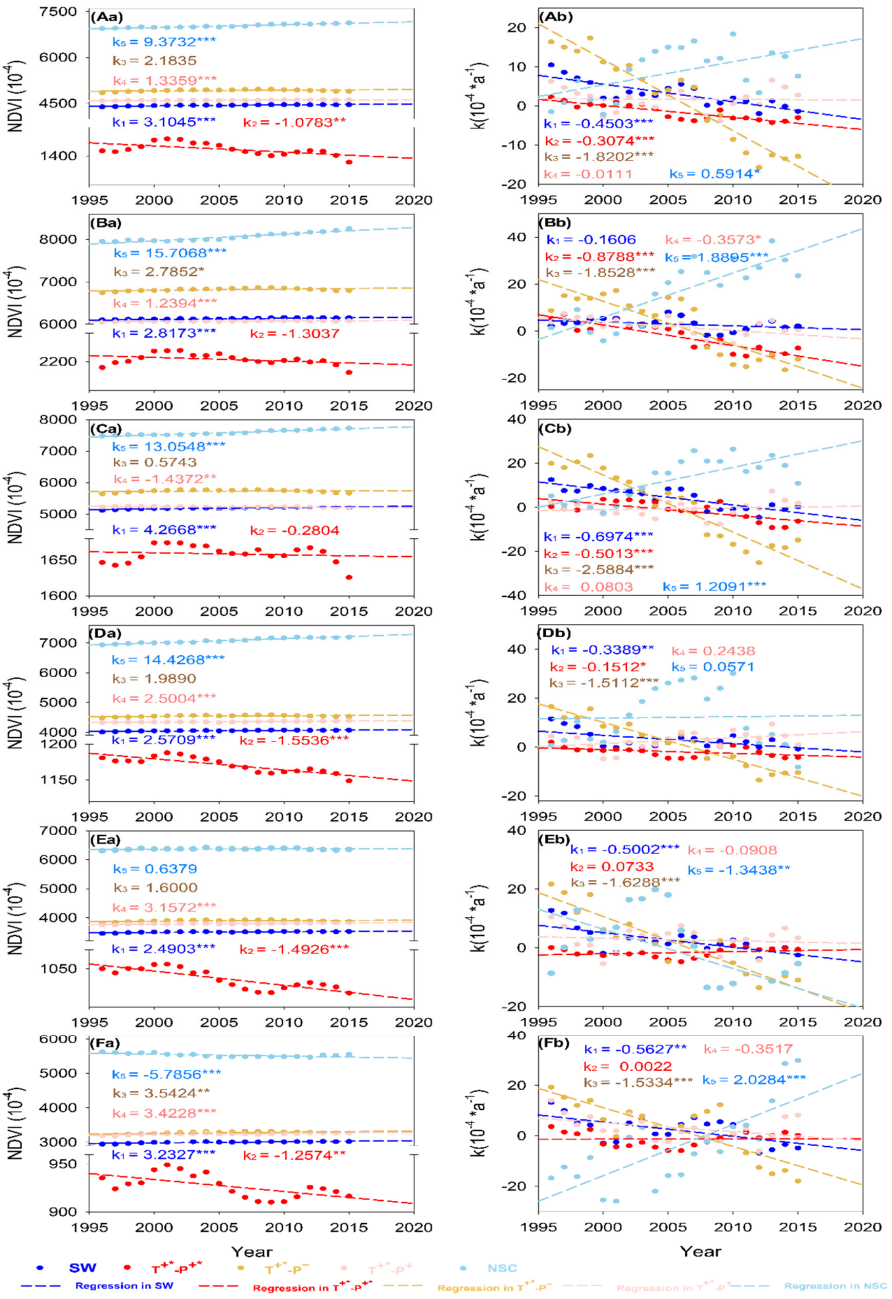

Figure 3. Interannual variation characteristics of *NDVI* and interannual trend k over 15 years of sliding. Capital letters (**A**–**F**) represent Mean, P_{100}, P_{75}, P_{50}, P_{25} and P_5, respectively, and small letters (**a**,**b**) refer to the *NDVI* and interannual trend k over 15 years of sliding. Numbers 1–5, respectively, represent the SW, T^{+*}-P^{+*}, T^{+*}-P^{-}, T^{+*}-P^{+} and NSC.

3.3. Correlation between Vegetation Changes and Climate in Core Areas

The six annual eigenvalues (Figure 4) in SW and T^{+*}-P^{-} areas were changed by temperature and precipitation strongly, which belong to $[T+P]^{+}$ type (Table 2) and had a significant positive correlation between temperature and precipitation above 0.70 ($p < 0.01$). When Mean, P_{100} and P_{75} were respectively in T^{+*}-P^{+*} area, they were $[T+P]^{+}$, and had a significant negative/positive correlation between the temperature/precipitation ($p < 0.01$); and the remaining annual value synthesis was changed by temperature (T) or temperature weakly (T^{-}), and had significant negative correlation between the temperature ($p < 0.05$). In the T^{+*}-P^{+} area, at P_{100} and P_5, it belongs to the changed by precipitation (P) or precipitation weakly (P^{-}), respectively, with a significant positive correlation between precipitation

($p < 0.05$); and at P_{75}, it belongs to the changed by temperature and precipitation weakly ($[T+P]^-$), with a negative correlation between both temperature and precipitation. When P50–P25 and Mean were changed by temperature (T) or temperature weakly (T^-), respectively, they were significantly positively correlated with the temperature ($p < 0.05$). In the NSC area, at P_5, it was changed by temperature weakly (T^-), and had a significant negative correlation between temperature ($p < 0.05$). At P_{25}, it was changed by temperature and precipitation strongly ($[T+P]^+$), with a significant positive correlation between both temperature and precipitation ($p < 0.01$). The remaining annual value synthesis was changed by temperature (T), and there was a significant positive correlation between the temperature ($p < 0.01$). The results showed that the precipitation was relatively large in the overall scope the SW region and the temperature increases, which could enhance the ability of photosynthesis of vegetation and promote the growth of plants. However, this phenomenon masked the fact that rising temperatures in T^{+*}-P^{+*} areas inhibit plant growth, because in T^{+*}-P^{+*} areas, the higher the temperature, the stronger the evaporation, even though there was an increase in rainfall at this time, the precipitation was less, ultimately limiting plant growth.

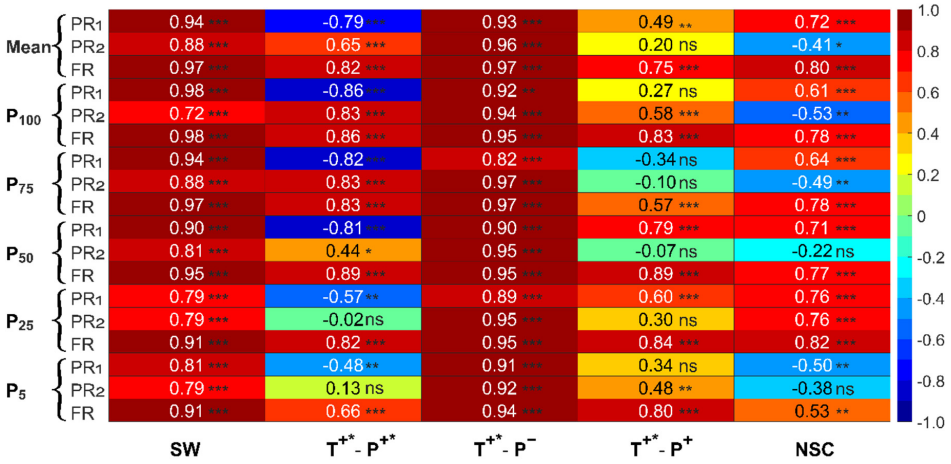

Figure 4. Correlation coefficients between *NDVI* and temperature and precipitation over 15 years of sliding. PR_1 represent partial correlation between *NDVI* and temperature; PR_2 represent partial correlation between *NDVI* and precipitation; FR represent multiple correlations between *NDVI* and temperature and precipitation. "*", "**", and "***" indicate the significance of $p < 0.1$, $p < 0.05$, and $p < 0.01$, respectively.

3.4. Change Trend of Correlation Coefficients between Vegetation and Climate Factors in Core Areas

The correlation between temperature (except P_{100} and P_{75}) increased, while the correlation between precipitation (except P_{50}) decreased; the results showed that in the whole SW region had different responses to climate factors in different periods, at P_{100}, P_{75} and P_{25} showed a decreasing trend, while Mean, P_{50} and P_5 showed an increasing trend (Figure 5). In the T^{+*}-P^{+*} area, the influence of temperature gradually decreased, while precipitation significantly increased, and the combined effect of the two shows a significant increasing trend. In T^{+*}-P^- area, the correlation between *NDVI* (except P_{75}) and climate factors decreased significantly at a rate of more than 0.06/(10a) ($p < 0.05$); and the correlation between temperature (except P_{100}) and precipitation (except P_{75}) decreased at a rate of more than 0.03/(10a), indicating that the correlation between the single factor and multiple correlation factor in T^{+*}-P^- area decreased. In T^{+*}-P^- area, the growth of vegetation was significantly increased by temperature, decreased by precipitation, and increased by both. In the NSC area, the correlation between *NDVI* and climate factors decreased significantly at a rate of more than 0.10/(10a); the correlation between temperature decreased significantly (except P_{100}), while the correlation between precipitation increased significantly, indicating that the

influence of temperature significantly reduced the vegetation, but significantly increased by the influence of precipitation, showing a significant downward trend under the combined influence of both.

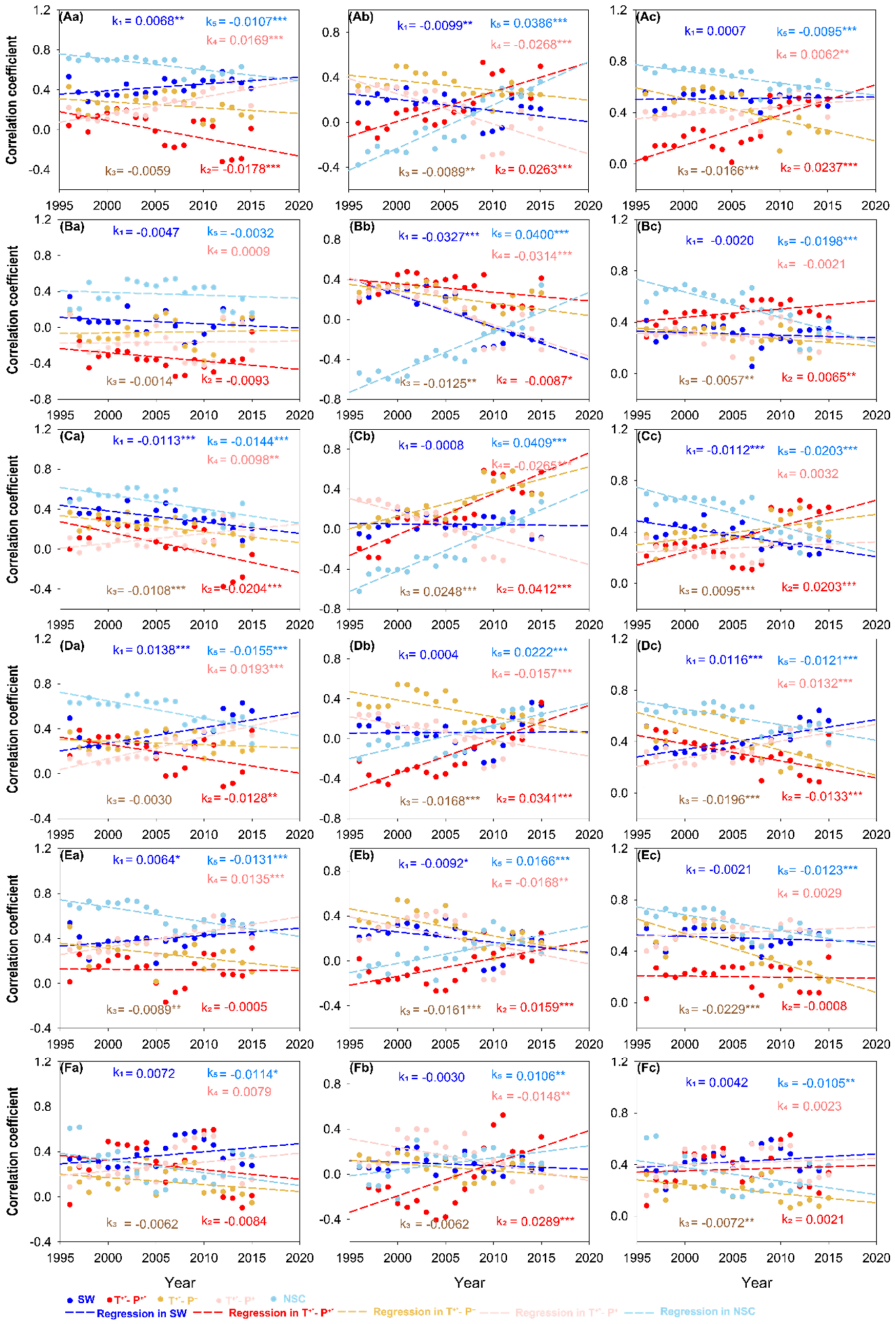

Figure 5. Change trend of the correlation coefficient between *NDVI* and temperature and precipitation over 15 years of sliding. Capital letters (**A**–**F**) represent Mean, P_{100}, P_{75}, P_{50}, P_{25} and P_5, respectively. Small letters (**a**–**c**) refer to the partial correlation coefficient and the multiple correlation coefficient between *NDVI* and temperature and precipitation. Numbers 1–5, respectively, represent the SW, T^{+*}-P^{+*}, T^{+*}-P^{-}, T^{+*}-P^{+} and NSC.1–5 respectively represent the SW, T^{+*}-P^{+*}, T^{+*}-P^{-}, T^{+*}-P^{+} and NSC. "*", "**", and "***" indicate the significance of $p < 0.1$, $p < 0.05$, and $p < 0.01$, respectively.

4. Discussion

4.1. Necessity of Analysis of Typical Climate Type Areas (Core Areas)

On the whole, the average annual temperature of the study area in the past 36 years showed an increasing trend (Figure 2a), and the area with a significant increase was about 98.10%, indicating that the temperature had been increasing continuously for more than 30 years, but not in the similar situation of global warming interruption (slowing or stagnating) [58,59], which was consistent with the research results of Shen [60], Zhu [61] and Duan [62] on the Qinghai–Xizang Plateau and its surrounding areas, was consistent with the rapid warming of global temperature reported by IPCC [27,43] in the past 30 years. The precipitation (Figure 2a) of the study area in the past 36 years had no significant change overall, showing a trend of "increased–decreased–increased" from east to west in space. The areas with increased precipitation (65.78%) were concentrated in the western and eastern of SW, while the areas with decreased precipitation were concentrated in the middle of the study area, including the western Yunnan-Guizhou Plateau, Hengduan Mountains and the southeast part of Qinghai–Xizang Plateau. Yang [63] pointed out that precipitation decreased in the southern and eastern parts of the Qinghai-Xizang Plateau, and increased in the central and western regions. According to the global precipitation climatology project (www.esrl.noaa.gov/psd/data/gridded/data.gpcp.html, accessed on 27 February 2021) and rainfall distribution in India (www.tropmet.res.in, accessed on 27 February 2021), the precipitation in the Himalayas decreased from 1979 to 2010, while that in the eastern Pamir increased; this further verified the changing trend of precipitation in the study area, whereas many studies have shown that vegetation growth was closely related to water and heat conditions, and climate change can jointly determine the long-term evolution of vegetation and ecosystem by redistributing climate factors in space and time [5,8,25]. Therefore, in order to improve the understanding of vegetation response to climate change, from the direction and significance of climate change trend, we identified four major types of climate change (T^{+*}-P^{+*}, T^{+*}-P^{+}, T^{+*}-P^{-} and NSC) in the SW. In this case, we may well explain the large regional differences in the response of vegetation growth to climate change [4,5,8,12]; for example, the response of vegetation activities to temperature in the growing season was positively regulated by precipitation, but with the continuous climate warming, if precipitation did not increase or even decrease, the decoupling or even inverse correlation between NDVI and temperature will occur [4].

4.2. Vegetation Characteristics of Different Stages in CAs

In the context of rapid global environmental change, vegetation change can be used to describe the interaction between environmental change and the terrestrial ecosystem [13], which was helpful in understanding the cycling mechanism of various elements within the ecosystem [10,64]. In this study, six annual eigenvalues (P_{100}, P_{75}, P_{50}, P_{25}, P_5 and Mean) of GIMMS NDVI were used to characterize vegetation growth conditions, which made up for the deficiency in current studies that annual maximum or average value of *NDVI* was used to represent vegetation growth status [5,8,25,40]. The order of annual average *NDVI* of the six annual values (Mean, P_{100}–P_5) in SW and CAs was basically: NSC > T^{+*}-P^{-} > T^{+*}-P^{+} > SW > T^{+*}-P^{+*}, and the maximum values reach 3.65–6.05 times of the minimum values, respectively, indicating that there was a considerable spatial heterogeneity of *NDVI* in different CAs in the study area, which may be due to the close relationship between vegetation growth and hydrothermal conditions, and climate change determines the long-term evolution of vegetation and ecosystem [5,8], climatic factors (hydrothermal conditions) have considerable spatial heterogeneity [65], which directly drive water cycle and energy cycle, making the response of vegetation growth to climate change had large regional differences. Generally speaking, the vegetation in the whole SW region increased significantly in the NSC, the T^{+*}-P^{-} area and the T^{+*}-P^{+} area, and there was a phenomenon of accelerated decrease (Browning) in the local area (T^{+*}-P^{+*} area), which was similar to that of most researchers [10,29,66,67] and Pan [29] pointed out the trend of global vegetation greening, but covered up the increase of vegetation browning in local areas; Zhang [10]

and Cui [66] found that *NDVI* in the Yellow River and Yangtze River Basins increased as a whole and decreased locally; Yao [67] research showed that the greening speed in arid areas may be slower than that in humid areas, which can also explain the result that NSC area in this study belongs to humid area, and its greening speed was the highest, while the relatively small results in the T^{+*}-P^{-} and T^{+*}-P^{+} areas.

Furthermore, we found that vegetation activity in the whole SW region and each CAs changed with time (Figure 3), and the turning point of the SW region, T^{+*}-P^{-} and T^{+*}-P^{+} areas was around 2005 (represented the period from 1991 to 2005), in which the growth rate of vegetation activity was larger before 2005, and slowed down after 2005. In the NSC area, the growth rate was about 2005, but the growth rate was accelerated after 2005. In the T^{+*}-P^{+*} area, the dividing time year was 2001 (representing the period from 1987 to 2001) and was increasing before 2001 and decreasing after 2001. Similarly, some studies had pointed out that the global terrestrial ecosystem was a net carbon sink in the 1980s and 1990s [68]), and the vegetation activity was greatly enhanced. Since the early 1990s, the global browning trend had gradually expanded and strengthened [29], and the browning trend of all latitudes in the Northern Hemisphere was increasing. During the 2000s, the vegetation productivity in most parts of the Southern Hemisphere began to decline, resulting in a significant decrease in global net primary productivity and *NDVI* in 2000s [19,69]. In the Northern Hemisphere and East Asia, the year 1997 was regarded as a turning year [70,71], and the trend of vegetation from greening to browning was found.

4.3. Main Climate Driving Types in CAs

Climate change determines the long-term evolution of vegetation and ecosystem [5,8], which controls 70% of the global vegetation growth and change, and is a key factor restricting global vegetation productivity [40,41,71]. In this study, we concluded that the growth of vegetation in the whole SW region and the CAs could be controlled by temperature and precipitation factors alone or jointly. In the SW and T^{+*}-P^{-} areas, the vegetation growth was strongly driven by temperature and precipitation ($[T+P]^{+}$), and both temperature and precipitation play a promoting role in vegetation growth, possibly because the continuous global warming can increase the duration of the vegetation growth period and enhance photosynthesis [3,72]; meanwhile, the increase of precipitation increases soil moisture to meet the needs of vegetation [19,21]. In the T^{+*}-P^{+*} area, it was mainly affected by the negative effect of temperature, with less precipitation, lower soil moisture content, higher temperature and faster evaporation, which exceeded the availability of water and inhibited the growth of vegetation [1,40]. In the T^{+*}-P^{+} area, the vegetation growth and climate factors were different in different periods, and the precipitation had a positive effect at P_{100} and P_5, the temperature had a positive effect at Mean, P_{50} and P_{25}, and the temperature and precipitation had a negative correlation at P_{75}. The positive effect of temperature was mainly driven the NSC area, and its positive effect was greater than the negative effect of precipitation. Due to the NSC area in the humid subtropical area (http://www.resdc.cn/data.aspx?DATAID=125, accessed on 1 December 2019), the rainfall is higher, and the soil water content is higher than the threshold value of vegetation response to rainfall, the positive effect of rainfall on vegetation is offset, and vegetation growth is inhibited [20]. The temperature increase can effectively improve the temperature of the environment around the vegetation, increase solar radiation, enhance photosynthesis, and promote the growth of vegetation [3].

4.4. Staged Response of Vegetation to Climate Change in CAs

The response of vegetation activity to climate change changes with time [4,8,28,29]. For example, some studies had pointed out that with the continuous warming of the climate, if the precipitation does not increase or even decrease, *NDVI* and temperature show decoupling or even reverse correlation [4], which made the response of vegetation growth to climate change more complex [18,40,41]. In this study, the response of six annual synthetic *NDVI* to climate factors in the T^{+*}-P^{+*} area and T^{+*}-P^{+} area (Figure 5) mainly showed an

increasing trend ($p < 0.05$), indicating that the influence of climate on *NDVI* showed an increasing trend. The single influence of being influenced by temperature or precipitation was completely opposite in the T^{+*}-P^{+*} area and T^{+*}-P^{+} area, which in the T^{+*}-P^{+*} area was gradually reduced by temperature and gradually increased by precipitation, while in the T^{+*}-P^{+} area was gradually increased by temperature and significantly decreased by precipitation, which was consistent with the research results of Cong [28] on grassland vegetation in the Qinghai–Xizang Plateau. It may be due to the T^{+*}-P^{+*} area in the semi-arid area of the plateau sub frigid zone (http://www.resdc.cn/data.aspx?DATAID=125, accessed on 1 December 2019); the precipitation is less, and the positive response to precipitation is enhanced due to the increase of temperature, which made the response of vegetation activity to precipitation stronger. The T^{+*}-P^{+} region is located in the sub frigid sub-humid region of the plateau, the temperate humid sub-humid region of the plateau and the humid region of the middle subtropics, and its precipitation is relatively large. With the increase of precipitation, the response of vegetation activity to temperature was more sensitive (the response of vegetation activity to temperature was greater). When the temperature rises, the influence of temperature gradually increased. The response of *NDVI* to climate factors in the T^{+*}-P^{-} area and the NSC area (Figure 5) showed a significant decreasing trend ($p < 0.05$), which indicated that *NDVI* was significantly affected by climate. In the T^{+*}-P^{-} area, the single influence of being influenced by temperature or precipitation was gradually reduced, while in the NSC area, it was gradually decreased by temperature and significantly increased by precipitation. It is possible that the correlation between temperature and *NDVI* was mainly positive in the T^{+*}-P^{-} area and NSC area (Figure 5), and gradually decreased with the extension of time, indicating that the promotion effect of temperature on vegetation growth gradually decreases, which was basically consistent with the performance of Piao [4] on the promoting effect of temperature on vegetation growth in the Northern Hemisphere (>30° N). The positive effect of precipitation on vegetation in T^{+*}-P^{-} areas decreased gradually, while the correlation between precipitation and *NDVI* in NSC area gradually changed from negative to positive, and the value gradually increased, indicating that with the continuous increase of temperature, the water demand for vegetation growth gradually increased, while the water fall in T^{+*}-P^{-} areas gradually decreased, and gradually approached the positive threshold of vegetation response to precipitation, the positive impact of precipitation on vegetation gradually decreased [20]. In contrast, the NSC area is located in the middle subtropical humid area (http://www.resdc.cn/data.aspx?DATAID=125, accessed on 1 December 2019) with the extension of time, the required water gradually increased, and the correlation gradually changed, and the vegetation needs more water to promote growth [20,28,31]. Finally, in the whole SW study area, with the extension of time, the influence of climate factors in the SW region decreased significantly at P_{75}, increased significantly at P_{50}, increased gradually at Mean and P_5, and decreased gradually at P_{100} and P_{25}. Our results showed that the partial correlation coefficient and complex correlation coefficient between *NDVI* and temperature or precipitation had considerable time variation, which indicated that the response of vegetation activity to climate change in SW and CAs changed with time, and the response to climate change in different growth stages (annual value synthesis) had different directionality. There are also relevant studies that showed that vegetation activities had different responses to climate change in different research periods [8,28,29,31,71].

5. Conclusions

Overall, we identified four major climate change types and nine corresponding different climate core areas across SW China in the past 30 years. We further showed that the vegetation in the SW region had become greener as a whole, but the rate of greening had gradually decreased, especially in T^{+*}-P^{+*} area, and the rate of decrease had continued to be significant, and the vegetation growth was found to be accelerating in the NSC area. Climate factors mainly control the vegetation growth in the SW region and the core areas, and different vegetation growth periods (P_{100}–P_5 and Mean) in the whole region and the

core areas had different regional and phased responses to climate change. Therefore, when we compare the response of different vegetation activity stages to climate change, more attention should be paid to clarifying the research period and the vegetation's growth stage.

Author Contributions: Conceptualization, M.W.; methodology, M.W.; software, M.W.; validation, M.W. and Z.A.; formal analysis, M.W.; investigation, M.W.; resources, M.W.; data curation, M.W.; writing—original draft preparation, M.W. and Z.A.; writing—review and editing, M.W. and Z.A.; visualization, M.W.; supervision, M.W.; project administration, M.W.; funding acquisition, M.W. All authors have read and agreed to the published version of the manuscript.

Funding: This research was funded by Chaozhou Special Fund for Human Resource Development, grant number 2022.

Institutional Review Board Statement: Not applicable.

Informed Consent Statement: Not applicable.

Data Availability Statement: The NDVI datasets used in our work can be freely accessed at https://ecocast.arc.nasa.gov/data/pub/GIMMS/, accessed on 18 November 2018. The climate data (CRU_TS4.02) were obtained from https://crudata.uea.ac.uk/cru/data/hrg/, accessed on 18 December 2018.

Conflicts of Interest: The authors declare no conflict of interest.

Appendix A

Core Area Screening Principles of Climate Change in Southwest China

(1) Homogeneity: according to the vegetation division (Figure 1b) obtained from the Resource and Environment Science and Data Center, as the classification judgment of homogeneity affected by climate change, the vegetation division and climate change types were superimposed to obtain 14 spatially explicit major sub-regions of climate change types by referring to Table A3 (Figure A1a).

(2) Typicality: according to the impact degree of climate change, the order of typicality was Intensity > Moderate > Mild > Slight degree. Furthermore, the climate impact degree of different climate change sub-regions can be obtained by superimposing the climate impact degree map of different climate change sub-regions (Figure A1b).

(3) Concentration: Based on the absolute value of the change rate ($|K|$) of temperature and precipitation, the area whose $|K|$ exceeds the 95% confidence upper limit of t-test was recorded as a typical area, and then the typical area of temperature and precipitation was superimposed, and the superimposed overlapping area was recorded as the core area. In the NSC area (the region with the least impact of climate change), the overlapping region of $|K|$ of temperature and precipitation, which was lower than the 95% confidence limit of t-test, was selected, indicating that it was less affected by climate (temperature and precipitation) change and relatively stable.

(4) Adjusted rules: based on the previous steps, some core areas were relatively scattered and had different sizes, which need to be further adjusted. The details were as follows:

① Considering the spatial distribution and size of different climate change sub-regions, the core area in this study was uniformly defined as 20 grids, and each grid was $0.25^\circ \times 0.25^\circ$ (about 25 km × 25 km).
② In the T^{+*}-P^- and T^{+*}-P^+ areas, the changing trend of temperature was mainly $|K|$, and the range of $|K|$ of precipitation was appropriately scaled.
③ When the overlapped significant regions and the regions with a high degree of climate impact were small, the distribution regions with a high degree of climate impact were the priority, and the core areas were selected by combining the two rules.
④ The core area initially screened out in IV and V areas were closely connected with the middle part of their contact boundary, so a specific area was re-screened out after merging IV and V areas as the core area of the two areas.

Appendix B

Table A1. Classification of climate change patterns.

Climate Change Types	Temperature	Precipitation
T^{+*}-P^{+*}	Significantly increased	Significantly increased
T^{+*}-P^{-}	Significantly increased	Decreased but not to a significant level
T^{+*}-P^{+}	Significantly increased	Increased but not to a significant level
NSC	Increased but not to a significant	Increased but not to a significant

Table A2. Criteria for grading the degree of climate impact in Southwest China.

Indicators	Classification	Criteria	Grade Evaluation
Variability	Low	$S\,(CV) < 0.95$	1
	High	$S\,(CV) > 0.95$	2
Probability	Small	$Pd < 0.95$	1
	Large	$Pd > 0.95$	2
Effect degree	Slight	—	4
	Mild	—	5
	Moderate	—	6
	Intensive	—	7

Table A3. Sub-regions of climate change types in Southwest China. Classification of vegetation zones: I, alpine vegetation region; II–V, respectively, represent the northwest region, west central region and northwest region of subtropical evergreen broad-leaved forest; and VI, tropical monsoon forest.

Climate Change Types	Vegetation Zones	Sub-Regions of Climate Change Types
T^{+*}-P^{+*}	I	T^{+*}-P^{+*}-I
T^{+*}-P^{-}	I	T^{+*}-P^{-}-I
	II	T^{+*}-P^{-}-II
	III	T^{+*}-P^{-}-III
	IV	T^{+*}-P^{-}-IV
	V	T^{+*}-P^{-}-V
	VI	T^{+*}-P^{-}-VI
T^{+*}-P^{+}	I	T^{+*}-P^{+}-I
	II	T^{+*}-P^{+}-II
	III	T^{+*}-P^{+}-III
	IV	T^{+*}-P^{+}-IV
	V	T^{+*}-P^{+}-V
	VI	T^{+*}-P^{+}-VI
NSC	VI	NSC-VI

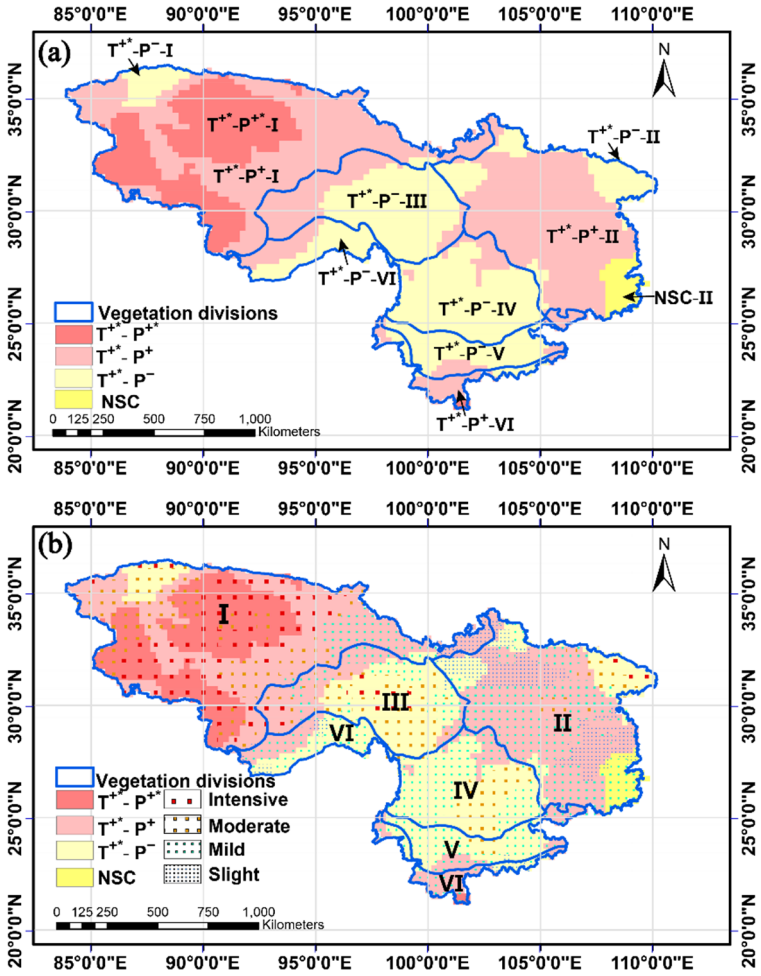

Figure A1. (**a**) The spatial distribution map of sub-regions of climate change and (**b**) the impact degree corresponding to sub-regions of climate change in Southwest China.

References

1. Li, P.; Peng, C.; Wang, M.; Luo, Y.; Li, M.; Zhang, K.; Zhang, D.; Zhu, Q. Dynamics of vegetation autumn phenology and its response to multiple environmental factors from 1982 to 2012 on Qinghai-Tibetan Plateau in China. *Sci. Total Environ.* **2018**, *637–638*, 855–864. [CrossRef] [PubMed]
2. Nemani, R.R.; Keeling, C.D.; Hashimoto, H.; Jolly, W.M.; Piper, S.C.; Tucker, C.J.; Myneni, R.B.; Running, S.W. Climate-driven increases in global terrestrial net primary production from 1982 to 1999. *Science* **2003**, *300*, 1560–1563. [CrossRef]
3. Piao, S.L.; Mohammat, A.; Fang, J.; Cai, Q.; Feng, J. NDVI-based increase in growth of temperate grasslands and its responses to climate changes in China. *Glob. Environ. Chang.* **2006**, *16*, 340–348. [CrossRef]
4. Piao, S.L.; Nan, H.; Huntingford, C.; Zeng, N.; Zeng, Z.; Chen, A. Evidence for a weakening relationship between interannual temperature variability and northern vegetation activity. *Nat. Commun.* **2014**, *5*, 5018. [CrossRef] [PubMed]
5. Piao, S.L.; Yin, G.D.; Tan, J.G.; Zeng, N.; Zeng, Z.Z.; Wang, Y.P. Detection and attribution of vegetation greening trend in China over the last 30 years. *Glob. Chang. Biol.* **2015**, *21*, 1601–1609. [CrossRef] [PubMed]
6. Piao, S.L.; Wang, X.H.; Park, T.; Tømmervik, H.; Nemani, R.R.; Myneni, R.B. Characteristics, drivers and feedbacks of global greening. *Nat. Rev. Earth. Environ.* **2020**, *1*, 14–27.
7. Lamchin, M.; Lee, W.K.; Jeon, S.W.; Wang, S.W.; Lim, C.H.; Song, C.; Sung, M. Long-term trend and correlation between vegetation greenness and climate variables in Asia based on satellite data. *Sci. Total Environ.* **2018**, *618*, 1089–1095. [CrossRef] [PubMed]
8. Lamchin, M.; Wang, W.; Lim, C.; Ochir, A.; Ukrainski, P.; Gebru, B.; Choi, Y.; Woo, S.; Lee, W. Understanding global spatio-temporal trends and the relationship between vegetation greenness and climate factors by land cover during 1982–2014. *Glob. Ecol. Conserv.* **2020**, *24*, e01299. [CrossRef]
9. Li, Y.; Gong, J.; Zhang, Y.; Gao, B. NDVI-Based Greening of Alpine Steppe and Its Relationships with Climatic Change and Grazing Intensity in the Southwestern Tibetan Plateau. *Land* **2022**, *11*, 975. [CrossRef]
10. Zhang, W.; Wang, L.C.; Xiang, F.F.; Qin, W.M.; Jiang, W.X. Vegetation dynamics and the relations with climate change at multiple time scales in the Yangtze River and Yellow River Basin, China. *Ecol. Indic.* **2020**, *110*, 105892. [CrossRef]

11. de Jong, R.; Schaepman, M.E.; Furrer, R.; de Bruin, S.; Verburg, P.H. Spatial relationship between climatologies and changes in global vegetation activity. *Glob. Chang. Biol.* **2013**, *19*, 1953–1964. [CrossRef] [PubMed]
12. Wen, Z.; Wu, S.; Chen, J.; Lü, M. NDVI indicated long-term interannual changes in vegetation activities and their responses to climatic and anthropogenic factors in the Three Gorges Reservoir Region, China. *Sci. Total Environ.* **2017**, *574*, 947–959. [CrossRef] [PubMed]
13. Li, H.; Liu, L.; Liu, X.; Li, X.; Xu, Z. Greening Implication Inferred from Vegetation Dynamics Interacted with Climate Change and Human Activities over the Southeast Qinghai-Tibet Plateau. *Remote Sens.* **2019**, *11*, 2421. [CrossRef]
14. Stefanidis, S.; Alexandridis, V. Precipitation and potential evapotranspiration temporal variability and their relationship in two forest ecosystems in Greece. *Hydrology* **2021**, *8*, 160. [CrossRef]
15. Zindros, A.; Radoglou, K.; Milios, E.; Kitikidou, K. Tree line shift in the Olympus Mountain (Greece) and climate change. *Forests* **2020**, *11*, 985. [CrossRef]
16. Seddon, A.W.R.; Macias-Fauria, M.; Long, P.R.; Benz, D.; Willis, K.J. Sensitivity of global terrestrial ecosystems to climate variability. *Nature* **2016**, *531*, 229. [CrossRef] [PubMed]
17. Pepin, N.; Bradley, R.S.; Diaz, H.F.; Wang, M.B.; Williamson, S.N.; Yang, D.Q. Elevation-dependent warming in mountain regions of the world. *Nat. Clim. Chang.* **2015**, *5*, 424–430.
18. Ganjurjav, H.; Gornish, E.S.; Hu, G.Z.; Schwartz, M.W.; Wan, Y.; Li, Y.; Gao, Q. Warming and precipitation addition interact to affect plant spring phenology in alpine meadows on the central Qinghai-Tibetan Plateau. *Agric. For. Meteorol.* **2020**, *287*, 107943. [CrossRef]
19. Piao, S.L.; Wang, X.; Ciais, P.; Zhu, B.; Wang, T.; Liu, J.I.E. Changes in satellite-derived vegetation growth trend in temperate and boreal Eurasia from 1982 to 2006. *Glob. Chang. Biol.* **2011**, *17*, 3228–3239. [CrossRef]
20. Guan, Q.; Yang, L.; Pan, N.; Lin, J.; Xu, C.; Wang, F.; Liu, Z. Greening and Browning of the Hexi Corridor in Northwest China: Spatial Patterns and Responses to Climatic Variability and Anthropogenic Drivers. *Remote Sens.* **2018**, *10*, 1270. [CrossRef]
21. You, G.; Arain, M.A.; Wang, S.; Zhang, X.H.; Gu, Y.Y.; Gao, J.X. The spatial-temporal distributions of controlling factors on vegetation growth in Tibet Autonomous Region, Southwestern China. *Environ. Res. Commun.* **2019**, *1*, 091003. [CrossRef]
22. Yuan, W.; Wu, S.Y.; Hou, S.G.; Xu, Z.W.; Lu, H.Y. Normalized Difference Vegetation Index-based assessment of climate change impact on vegetation growth in the humid-arid transition zone in northern China during 1982–2013. *Int. J. Climatol.* **2019**, *39*, 5583–5598. [CrossRef]
23. Zhang, Y.; Zhu, Z.; Liu, Z.; Zeng, Z.; Ciais, P.; Huang, M.; Liu, Y.; Piao, S.L. Seasonal and interannual changes in vegetation activity of tropical forests in Southeast Asia. *Agric. For. Meteorol.* **2016**, *224*, 1–10. [CrossRef]
24. Wang, X.H.; Piao, S.L.; Ciais, P.; Li, J.S.; Friedlingstein, P.; Koven, C.D.; Chen, A.P. Spring temperature change and its implication in the change of vegetation growth in North America from 1982 to 2006. *Proc. Natl. Acad. Sci. USA* **2011**, *108*, 1240–1245. [CrossRef]
25. Wu, D.; Zhao, X.; Liang, S.; Zhou, T.; Huang, K.; Tang, B.; Zhao, W. Time-lag effects of global vegetation responses to climate change. *Glob. Chang. Biol.* **2015**, *21*, 3520–3531. [CrossRef]
26. Zhao, L.; Dai, A.; Dong, B. Changes in global vegetation activity and its driving factors during 1982–2013. *Agric. For. Meteorol.* **2018**, *249*, 198–209. [CrossRef]
27. IPCC. Climate Change 2021: The physical science basis. In *Contribution of Working Group, I to the Sixth Assessment Report of the Intergovernmental Panel on Climate Change*; Cambridge University Press: Cambridge, UK, 2021.
28. Cong, N.; Shen, M.G.; Yang, W.; Yang, Z.; Zhang, F.G.; Piao, S.L. Varying responses of vegetation activity to climate changes on the Tibetan Plateau grassland. *Int. J. Biometeorol.* **2017**, *61*, 1433–1444. [CrossRef]
29. Pan, N.Q.; Feng, X.M.; Fu, B.J.; Wang, S.; Ji, F.; Pan, S. Increasing global vegetation browning hidden in overall vegetation greening: Insights from time-varying trends. *Remote Sens. Environ.* **2018**, *214*, 59–72. [CrossRef]
30. Hansen, J.; Ruedy, R.; Sato, M.; Lo, K. Global surface temperature change. *Rev. Geophys.* **2010**, *48*, 1–29. [CrossRef]
31. Wang, H.; Liu, D.; Lin, H.; Montenegro, A.; Zhu, X. NDVI and vegetation phenology dynamics under the influence of sunshine duration on the Tibetan plateau. *Int. J. Climatol.* **2015**, *35*, 687–698. [CrossRef]
32. Zhang, J.; Zhang, Y.; Qin, S.; Wu, B.; Wu, X.; Zhu, Y.; Shao, Y.; Gao, Y.; Jin, Q.; Lai, Z. Effects of seasonal variability of climatic factors on vegetation coverage across drylands in northern China. *Land Degrad. Dev.* **2018**, *29*, 1782–1791.
33. Yuan, J.J.; Guo, J.Y.; Niu, Y.P.; Zhu, C.C.; Li, Z. Mean Sea Surface Model over the Sea of Japan Determined from Multi-Satellite Altimeter Data and Tide Gauge Records. *Remote Sens.* **2020**, *12*, 4168. [CrossRef]
34. Li, X.C. *Historical Geography: Geopolitics, Regional Economy and Culture*; Peking University Press: Beijing, China, 2004; pp. 79–93. (In Chinese)
35. You, Q.; Chen, D.; Wu, F.; Pepin, N.; Cai, Z.; Ahrens, B.; Jiang, Z.; Wu, Z.; Kang, S.; Amir, A.K. Elevation dependent warming over the Tibetan Plateau: Patterns, mechanisms and perspectives. *Earth-Sci. Rev.* **2020**, *210*, 103349. [CrossRef]
36. Zhao, W.J. Extreme weather and climate events in China under changing climate. *Natl. Sci. Rev.* **2020**, *7*, 938–943. [PubMed]
37. Wang, M.; Jiang, C.; Sun, O.J. Spatially differentiated changes in regional climate and underlying drivers in southwestern China. *J. For. Res.* **2022**, *33*, 755–765.
38. IPCC. *Special Report on Global Warming of 1.5 °C*; Cambridge University Press: Cambridge, UK, 2018.
39. China Meteorological Administration. *Blue Book on Climate Change in China 2020*; Science Press: Beijing, China, 2020.

40. Wang, H.; Liu, H.; Cao, G.; Sanders, N.J.; Classen, A.T.; He, J.S. Alpine grassland plants grow earlier and faster but biomass remains unchanged over 35 years of climate change. *Ecol. Lett.* **2020**, *23*, 701–710. [CrossRef]
41. Zheng, Z.T.; Zhu, W.Q.; Zhang, Y.J. Seasonally and spatially varied controls of climatic factors on net primary productivity in alpine grasslands on the Tibetan Plateau. *Glob. Ecol. Conserv.* **2020**, *21*, e00814. [CrossRef]
42. Fu, Y.; Zhao, H.; Piao, S.L.; Peaucelle, M.; Peng, S.; Zhou, G.; Ciais, P.; Huang, M.T.; Menzel, A.; Penuelas, J.; et al. Declining global warming effects on the phenology of spring leaf unfolding. *Nature* **2015**, *526*, 104–107.
43. IPCC. *Climate Change 2013: The Physical Science Basis: Summary for Policymakers*; Cambridge University Press: Cambridge, UK, 2013.
44. Harris, I.; Osborn, T.; Jones, P.; Lister, D. Version 4 of the CRU TS monthly high-resolution gridded multivariate climate dataset. *Sci. Data* **2020**, *7*, 109.
45. Buermann, W.G.; Forkel, M.; O'Sullivan, M.; Sitch, S.; Friedlingstein, P.; Haverd, V. Widespread seasonal compensation effects of spring warming on northern plant productivity. *Nature* **2018**, *562*, 110–115. [PubMed]
46. Knott, G.D. *Interpolating Cubic Splines*; Springer Science & Business Media: Berlin, Germany, 2012; pp. 1–244.
47. Kang, S.C.; Xu, Y.W.; You, Q.L.; Flugel, W.A.; Pepin, N.; Yao, T.D. Review of climate and cryospheric change in the Tibetan Plateau. *Environ. Res. Lett.* **2010**, *5*, 015101. [CrossRef]
48. Morice, C.P.; Kennedy, J.J.; Rayner, N.A.; Winn, J.P.; Hogan, E.; Killick, R.E.; Dunn, R.J.H.; Osborn, T.J.; Jones, P.D.; Simpson, I.R. An updated assessment of near-surface temperature change from 1850: The HadCRUT5 dataset. *J. Geophys. Res. Atmos.* **2020**, *126*, e2019JD032361. [CrossRef]
49. Grosso, S.D.; Parton, W.J.; Derner, J.; Chen, M.; Compton, J.T. Simple models to predict grassland ecosystem C exchange and actual evapotranspiration using NDVI and environmental variables. *Agric. For. Meteorol.* **2018**, *249*, 1–10. [CrossRef]
50. Yin, L.; Wang, X.; Feng, X.; Fu, B.; Chen, Y. A Comparison of SSEBop-Model-Based Evapotranspiration with Eight Evapotranspiration Products in the Yellow River Basin, China. *Remote Sens.* **2020**, *12*, 2528. [CrossRef]
51. Huang, M.; Piao, S.L.; Janssens, I.A.; Zhu, Z.; Wang, T.; Wu, D.; Ciais, P.; Myneni, R.B.; Peaucelle, M.; Peng, S.S.; et al. Velocity of change in vegetation productivity over northern high latitudes. *Nat. Ecol. Evol.* **2017**, *1*, 1649–1654. [CrossRef] [PubMed]
52. Gong, P.; Li, X.; Wang, J.; Bai, Y.; Zhou, Y. Annual maps of global artificial impervious area (GAIA) between 1985 and 2018. *Remote Sens. Environ.* **2020**, *236*, 111510. [CrossRef]
53. Li, X.P.; Wang, L.; Guo, X.Y.; Chen, D.L. Does summer precipitation trend over and around the Tibetan Plateau depend on elevation? *Int. J. Climatol.* **2017**, *37*, 1278–1284. [CrossRef]
54. Gonzalez, P.; Neilson, R.P.; Lenihan, J.M.; Raymond, J.D. Global patterns in the vulnerability of ecosystems to vegetation shifts due to climate change. *Glob. Ecol. Biogeogr.* **2010**, *19*, 755–768. [CrossRef]
55. IPCC. Climate change 2007: The physical science basis. In *Contribution of Working Group I to the Fourth Assessment Report of the Intergovernmental Panel on Climate Change*; Cambridge University Press: Cambridge, UK; New York, NY, USA, 2017.
56. Chen, Y.H.; Li, X.B.; Shi, P.J. Variation in NDVI Driven by Climate Factors Across China, 1983–1992. *Chin. J. Plant. Ecol.* **2001**, *25*, 716–720. (In Chinese)
57. Maimaiti, A.; Rusuli, Y.; He, H.; Abudukerimu, B. Spatio-temporal characteristics of vegetation water use efficiency and its relationship with climate factors in Tianshan Mountains in Xinjiang from 2000 to 2017. *Chin. J. Plant. Ecol.* **2019**, *43*, 490–500. (In Chinese)
58. Zhu, X.; Dong, W.; Wei, Z.; Guo, Y.; Gao, X.; Wen, X.; Yang, S.; Zheng, Z.; Yan, D.; Zhu, Y.; et al. Multi-decadal evolution characteristics of global surface temperature anomaly data shown by observation and CMIP5 models. *Int. J. Climatol.* **2017**, *38*, 1533–1542. [CrossRef]
59. Kosaka, Y.; Xie, S. Recent global-warming hiatus tied to equatorial pacific surface cooling. *Nature* **2013**, *501*, 403–407. [CrossRef] [PubMed]
60. Shen, M.G.; Zhang, G.; Cong, N.; Wang, S.; Kong, W.; Piao, S.L. Increasing altitudinal gradient of spring vegetation phenology during the last decade on the Qinghai–Tibetan Plateau. *Agric. For. Meteorol.* **2014**, *189–190*, 71–80. [CrossRef]
61. Zhu, X.; Wei, Z.; Dong, W.; Wen, X.; Zheng, Z.; Chen, G.; Liu, Y. Projected temperature and precipitation changes on the Tibetan Plateau: Results from dynamical downscaling and CCSM4. *Theor. Appl. Climatol.* **2019**, *138*, 861–875. [CrossRef]
62. Duan, J.P.; Li, L.; Chen, L.; Zhang, H.X. Time-dependent warming amplification over the Tibetan Plateau during the past few decades. *Atmos. Sci. Lett.* **2020**, *21*, e998. [CrossRef]
63. Yang, K. Observed regional climate change in Tibet over the last decades. In *Regional Climate and Climate Change in the Region of Tibet*; Distributed by Oxford University Press: Oxford, UK, 2017.
64. Shen, Q.; Gao, G.; Han, F.; Xiao, F.; Ma, Y.; Wang, S.; Fu, B. Quantifying the effects of human activities and climate variability on vegetation cover change in a hyper-arid endorheic basin. *Land Degrad. Dev.* **2018**, *29*, 3294–3304. [CrossRef]
65. Piao, S.L.; Ciais, P.; Huang, Y.; Yu, Y.Q.; Zhang, T.Y.; Fang, J.Y. The impacts of climate change on water resources and agriculture in China. *Nature* **2010**, *467*, 43–51. [CrossRef]
66. Cui, L.; Wang, L.; Qu, S.; Singh, R.P.; Lai, Z.; Yao, R. Spatiotemporal extremes of temperature and precipitation during 1960–2015 in the Yangtze River Basin (China) and impacts on vegetation dynamics. *Theor. Appl. Climatol.* **2019**, *136*, 675–692. [CrossRef]
67. Yao, R.; Wang, L.; Huang, X.; Chen, X.X.; Liu, Z.J. Increased spatial heterogeneity in vegetation greenness due to vegetation greening in mainland China. *Ecol. Indic.* **2019**, *99*, 240–250. [CrossRef]

68. Schimel, D.S.; House, J.I.; Hibbard, K.A.; Scholes, R.J.; Steffen, W.L.; Wirth, C. Recent patterns and mechanisms of carbon exchange by terrestrial ecosystems. *Nature* **2001**, *414*, 169–172. [CrossRef]
69. Zhao, M.; Running, S.W. Drought-induced reduction in global terrestrial net primary production from 2000 through 2009. *Science* **2010**, *329*, 940–943. [CrossRef]
70. Park, H.S.; Sohn, B.J. Recent trends in changes of vegetation over East Asia coupled with temperature and rainfall variations. *J. Geophys. Res.* **2010**, *115*, D14101. [CrossRef]
71. Kong, D.D.; Zhang, Q.; Singh, V.P.; Shi, P.J. Seasonal vegetation response to climate change in the northern hemisphere (1982–2013). *Global Planet Chang.* **2017**, *148*, 1–8. [CrossRef]
72. Lehnert, L.W.; Wesche, K.; Trachte, K.; Reudenbach, C.; Bendix, J. Climate variability rather than overstocking causes recent large scale cover changes of Tibetan pastures. *Sci. Rep.* **2016**, *6*, 24367. [CrossRef] [PubMed]